High density nanoparticle Mn-Zn ferrite synthesis, characterisation and magnetic properties

R.B. Tangsali* and J.S. Budkuley

Department of Physics,
Department of Chemistry,
Goa University,
Taleigao Plateau, Goa 403206, India
E-mail: rbtangsali@ubnigoa.ac.in
E-mail: yaksha16@rediffmail.com
E-mail: jsbudkuley@rediffmail.com
*Corresponding author

S.H. Keluskar

Department of Physics,
P.E.S.S.R.S.N. College of Arts and Science,
Farmagudi, Goa 403401, India
E-mail: shpk@rediffmail.com

G.K. Naik

Department of Chemistry,
S.P. Chowgule. College of Arts and Science,
Margao, Goa 403601, India
E-mail: ganpatnaik@rediffmail.com

S.C. Watave

Department of Physics,
Gogate Gogalekar College,
Ratnagari, Maharashtra, India
E-mail: Shrikantwatawe@yahoo.com

Abstract: The amazing magnetic properties exhibited by nanoparticles Mn-Zn ferrites and their promising technological and medical applications have attracted much interest in recent years. Nanoparticle $Mn_x\ Zn_{(1-x)}\ Fe_2O_4$ spinel ferrites with x = 0.6/0.63/0.65/0.67/0.7 were synthesised by the nitrilotriacetate precursor method employing microwave combustion synthesis. Powder X-ray diffractometry (XRD) confirmed the formation of the ferrite phase in all samples. IR analysis was done to verify formation of spinel structure. Elemental analysis using EDS confirmed the nanoparticle composition. The crystallite size was calculated from peak widths using the Scherrer formula, yielding a size in the range of 10–25 nm. Transmission electron microscopy was also performed on the samples to testify formation of nanosized crystallites in the sample. Saturation magnetisation (Mr), retentivity (Ms) and coercivity (Hc) measurements were carried out on the samples using standard hysteresis

loop tracer equipment. The saturation magnetisation values were found to be in the range of 58.6–63.2 emu/g with very low values for (Mr/Ms). Variation of specific magnetisation with temperature and Curie temperature measurements were carried out using pulse field AC susceptibility measuring equipment. These measurements indicated formation of single domain (SD) material with dependence of Curie temperature on Zn concentration. The density of the samples was found to be high.

Keywords: nanoparticle; precursor method; ferrites; magnetic properties; density; superparamagnetism; hysteresis.

Reference to this paper should be made as follows: Tangsali, R.B., Budkuley, J.S., Keluskar, S.H., Naik, G.K. and Watave, S.C. (2011) 'High density nanoparticle Mn-Zn ferrite synthesis, characterisation and magnetic properties', *Int. J. Nanotechnol.*, Vol. 8, Nos. 10/11/12, pp.948–962.

Biographical notes: R.B. Tangsali completed his BSc (Physics) degree in 1979 from Dhempe College of Arts and Science Panjim, Goa, India, then affiliated to Bombay university. He obtained MSc in Physics with Electronics as special subject in the year 1981 from Centre of Post Graduate Instructions and Research Panjim, Goa, India, of Bombay University. In 1981 he joined as a Lecturer at Department of Physics, Dhempe College of Arts and Science, Panjim, Goa. He was conferred with PhD Degree in the year 1990 by Bombay University in Physics for his work on Mixed Valence Cerium compounds in Theoretical Physics carried out under the supervision R.B. Prabhu. In the year 1990 he joined department of Physics, Goa University, of Goa, India. He started Experimental work in the year 1994. Since then he has worked on magnetic materials, electroceramics, ferroelectrics, and dielectric materials. He has been in nanomagnetic materials since 2002 and presently is interested in luminance of nanomaterials and magnetic metamaterials. Currently working at Goa University is a life member of Indian Physics Association and Thermal Society of India. He is a recognised PhD guide, involved in Post graduate teaching as well as MPhil and PhD supervision.

Jayant S. Budkuley, MSc, PhD, graduated from Bombay University and obtained Doctorate for his thesis on Metal Ion- Sulphur Dioxide- Hydrazine Hydrate System, from the same University. He worked as Lecturer in Physical Chemistry in Smt. Parvatibai Chowgule College, Margao, Goa (India), and then joined Goa University, India. He has been Professor of Physical Chemistry, Dean of Faculty of Natural Sciences in this University. His field of interests has been- synthesis of magnetic materials, electroless plating, transition metal complexes and electrode-catalysis.

S.H. Keluskar graduated in 1984 and did his Masters in Physics in 1986 joined Department of Physics, P.E.S's SRSN College of Arts and Science, Goa, as an Lecturer in 1986 completed his MPhill degree and received his PhD while in service from Goa University Goa, India for his work on nanomagnetic materials under the supervision of R.B. Tangsali, in the year 2007. Currently, he is Associate Professor, in the same college affiliated to Goa University. His research is mainly focused on experimental work in Nano-Magnetic Materials. He has published eight research papers in refereed Journals. He has also completed his MPhil studies in Solid State Physics.

G.K. Naik, Associate Professor, in Department of Chemistry, at Smt. Parvatibai Chowgule College of Arts and Science, Margao Goa, India, graduated in 1986 in the subject of Chemistry, from Bombay University. He obtained his Masters Degree in 1988 in the area of Physical Chemistry from Bombay University.

He was conferred upon with PhD degree by Goa University, Goa, India for his research work on synthesis of metal nitrilotriacetate salts under the supervision of J.S. Budkuley. Presently he is working on synthesis and Characterisation of nanoparticle mixed ferrites and other nano materials. He is a life member of IANCAS society of BARC India.

S.C. Watave, Associate Professor in Physics at Gogate Jogalekar College, Ratnagiri, India. Graduated in 1982 and obtained a Master Degree in 1984 in the area of Materials Sciences and obtained the PhD degree in soft magnetic materials from Shivaji University, Kolhapur, India and presently working on synthesis and functionalisation of nano magnetic materials specifically for biological applications. A life member of Instruments society of India, Materials research society, Magnetic Society of India, Indian Association of Physics Teachers. He holds the charge of research cell in his institution.

1 Introduction

Ferrites are basically ceramic materials which are dark grey or black in colour when processed for applications in bulk form. These are ferromagnetic materials having formula MFe_2O_4, chemically inert, with M, a 3d metallic ion. Modern soft ferrites possess cubic spinel structure. Conventionally sintered soft ferrites are produced in solid bulk form which contains crystals typically of size ranging between 10 μm to 20 μm or more in dimension. These are produced by ceramic method or by other chemical methods like hydrothermal method, co-precipitation method etc. These crystals contain domains in which molecular magnets are already aligned. These materials exhibit high magnetic alignment and low conductivity and therefore find applications in power electronics, communication, and deflection yokes etc. where eddy current losses must be maintained low. It has been known for quite some time that the cation distribution in ferrites and their physical properties can be changed by choice of appropriate preparative conditions, thermal treatments, cationic substitutions, as well as by reducing the grain size of the basic green bodies prepared, to nanometre size [1–6]. Thus in addition to finite size effects, the inter-particle interaction effects, surface anomalies, lattice distortions introduced due to nanometre size grains and increase in surface to volume ratio make nanoparticle ferrites display a variety of exclusive magnetic properties. It is for this reason the study of these systems has attracted the attention of large number of researchers in recent years [2–12].

These particles when dispersed in liquids give rise to magnetic liquids widely used in technological devices as acceleration sensors, pressure assisted shock absorbers, magneto-optical modulators etc. when inserted in biological cells can be used as nanoscaled magnetic probes for local rheological investigations. When impregnated in malignant cells, can be used in hyperthermia causing death of malignant cells in tumours. These nanoparticles can be used in magneto responsive gels. It can also be used for ultra high magnetic information storage by dispersing in solid matrix. In MRI imaging, these are used as contrast agents. The most suitable ferrite preferred for these new technological applications are Mn-Zn ferrites. Mn-Zn ferrites belong to a class of mixed spinel ferrites are preferred in various applications due to high saturation magnetisation, low power loss, high permeability and high resistivity. It is well known that ferrites in

general are burdened with imperfections of various types. Thus it becomes essential to develop new methods and technologies to reduce the imperfections in these materials so that miniaturisation can be achieved with remarkable improvement in efficiency and power loss.

A ferrite nanoparticle with few unit cells exhibits two-fold magnetic behaviour. The particle magnetisation cannot be considered as uniform throughout the entire volume. The particles are made up of a well ordered core and a surface shell with disordered spins [13]. This could be due to the lattice distortions that occur at the surface of the nanoparticles. The additional contribution to high field magnetisation at low temperatures is attributed to disordered surface spin shell of the particles [14]. In the bulk material, the temperature dependence of magnetisation is determined by spin wave excitations. The surface effects in a nanoparticle arise due to lack of coordination of the surface ions due to large number of broken exchange bonds at the surface of the particle which results in frustration and spin disorder which increase with decreasing grain size. These two effects are expected to bring down the saturation magnetisation of the nanomaterial with decreasing particle size. Another parameter which can have a remarkable effect on the magnetisation of the particle is the width or the thickness of the disordered spin shell which may be directly related to the method of sample preparation. Nanoparticle ferrite material produced by high speed ball milling is found to exhibit low values for saturation magnetisation [15,16]. Thus a need of adopting appropriate preparative method with favourable modifications was felt necessary for possible enhancement of operational properties of Mn-Zn ferrite materials.

Porosity is a major factor that plays vital role when it comes to application of magnetic materials in bulk form. Powdered ferrites produced by conventional techniques do not adequately satisfy the requirement of small grain size. These powders on sintering produce bulk material with large porosity and nonuniform microstructure, which hampers the material performance. To overcome some of these discrepancies, bulk material can be prepared by sintering Mn-Zn nanoparticles, obtained by nitrilotriacetate precursor method [17] using modified microwaves based auto combustion technique.

Microwave heating is highly different from the conventional heating. In the conventional straightforward method of chemical synthesis, conductive heating with an external heat source is utilised. This is highly inefficient method for transferring heat energy into the reaction system. It depends on convection currents set up in the reactants, their thermal conductivity as well as reaction temperature of the container. As the heat penetrates in the material being heated from outer surface, a temperature gradient is developed within the sample. This does gives rise to local overheating which can lead to product, substrate or reagent decomposition prior to the start of reaction. In microwave radiated reactants heating is due to direct coupling of microwave energy with the molecules of reactants which is more efficient. Microwave heating is also responsible for enhancing the rate of reaction in chemical synthesis. The rate enhancement is possible in three different ways. Thermal effects (kinetics), specific thermal microwave effects and specific non-thermal microwave effects [18,19].

Thus due to microwave heating the possible existence of large temperature gradients in the precursor complex is ruled out. The material obtained by this process is homogeneous and of high purity and nearly free from agglomeration. In this paper we present the data collected on high quality nanoparticle $Mn_x\ Zn_{(1-x)}Fe_2O_4$ spinel ferrite material (x = 0.60/0.63/0.65/0.67/0.70) prepared using nitrilotriacetate precursor method employing microwave combustion synthesis. The nanomaterial synthesised exhibits high

density, super paramagnetic behaviour with high saturation magnetisation, low value for square ness and nearly zero hysteresis loss in some samples.

2 Experimental

Nanoparticle Mn-Zn ferrite materials $Mn_x\ Zn_{(1-x)}\ Fe_2O_4$ with x = 0.60, 0.63, 0.65, 0.67, 0.70 were synthesised using nitrilotriacetae precursor method adopting microwaves to stimulate auto combustion. The samples were prepared by mixing aqueous solution of metal salts in stoichiometric quantities and aqueous solution of dihydrazinium nitrilotriacetate [20]. Nitrilotriacetate hydrazinate precursors of mixed metal ions, so formed in solution were dried using microwaves. This initially resulted in a thick yellowish-brown coloured paste. The paste was then spread in a microwavable flat container and exposed to microwaves for further drying until combustion starts inside the microwave oven. The dried mass keeps burning slowly with a dark reddish coloured low flame with evolution of thick grey coloured fumes. The residue obtained is mixed with mortar and pestle on cooling, this is then exposed to microwaves for completion of the auto combustion process. The dry metal oxides obtained after auto combustion form the nanoparticle Mn-Zn ferrite samples. These powdered samples were then used for the characterisation and magnetic measurements.

Structure analysis and spinel phase identification were carried out by conventional X-ray diffraction (XRD) using Phillips X-ray diffractometer model X-pert. PRO PANalytical with Cu $K\alpha_1$ radiation having wavelength $\lambda = 1.54183$ AU for all the samples. FTIR absorption spectra were recorded using Shimadzu FTIR 8900 spectrometer. Estimation of metal ions Mn, Zn, Fe and O was carried out by Energy Dispersive Absorption of X-rays (EDAX) analysis using JEOL Model 840(SEM) scanning electron microscope. Transmission electron microscopy (TEM) was employed to confirm formation of ultra fine size material. TEM micrographs were taken on Philips model CM 200 transmission electron microscope. The ultra fine powders were pressed into pellets of the size 10 mm diameter and of thickness ranging between 2 mm and 3 mm by applying a pressure of 75 tons for 5 min. Saturation magnetisation measurements were carried out on the samples using standard hysteresis loop tracer equipment.

Magnetic measurements on the samples were carried out on different sophisticated instruments. Measurements to obtain temperature dependence of magnetisation and field dependence of magnetisation, at low temperatures on the nanoparticle $Mn_{0.67}Zn_{0.33}\ Fe_2O_4$ sample were carried out on Quantum Design MPMS-xl7 SQUID magnetometer with a maximum field of 50000 Oe. The room temperature data on magnetic properties namely retentivity $\mathbf{M_r}$ saturation magnetisation $\mathbf{M_s}$ squareness $\mathbf{M_r/M_s}$ and coercivity $\mathbf{H_c}$ of the nanoparticle samples was obtained on EV series vibrating sample magnetometer (VSM) model EV-5 from ADE US. Temperature dependent specific magnetisation data for the samples was recorded on automated standard pulse field magnetisation setup. The estimates of Curie temperature were obtained from these measurements. The density values for the samples were computed by following standard pyknometric method of measurement.

3 Results and discussion

3.1 X-ray diffraction

X-ray diffraction patterns obtained for powdered samples $Mn_x Zn_{(1-x)} Fe_2O_4$ with x = 0.6, 0.63, 0.65, 0.67, 0.7 are as shown in Figure 1. The d_{hkl} and 2θ values obtained for the samples when compared with the values reported in the literature (JCPDS files), were found to be in excellent agreement. Table 1 gives the lattice constant values calculated for the samples.

Figure 1 XRD patterns of as prepared (a) $Mn_{0.6}Zn_{0.4}Fe_2O_4$, (b) $Mn_{0.63}Zn_{0.37}Fe_2O_4$, (c) $Mn_{0.65}Zn_{0.35}Fe_2O_4$, (d) $Mn_{0.67}Zn_{0.33}Fe_2O_4$ samples (e) $Mn_{0.7}Zn_{0.3}Fe_2O_4$ samples (see online version for colours)

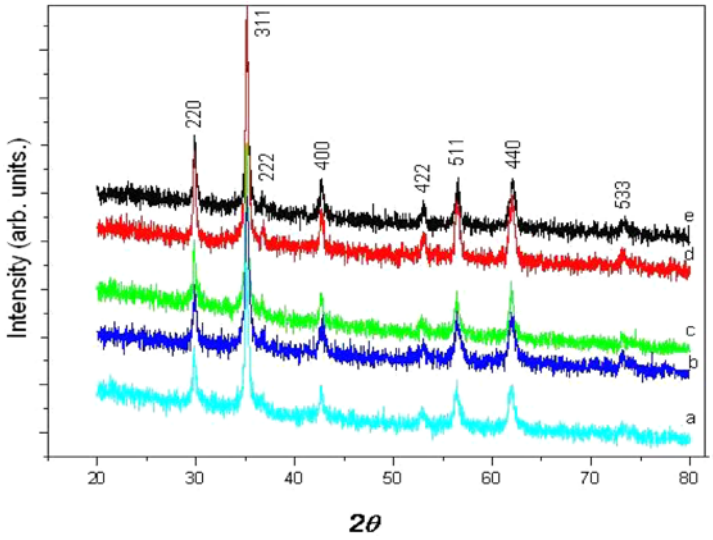

Table 1 Lattice constant variation with Zn concentration in $Mn_x Zn_{(1-x)} Fe_2O_4$

Mn Conc. x	0.60	0.63	0.65	0.67	0.70
Lattice Constant Å	8.45	8.452	8.454	8.457	8.461

The Zn concentration in Mn-Zn ferrite is known to have noticeable influence on the lattice parameter and cation distribution. The overall cation distribution is a consequence of two competing processes:

- the strong chemical affinity of certain cations to occupy either A- or B-sites
- the metastable cation distribution in nanoparticles which becomes much more complex when the stoichiometry is changed [20].

This normally arises when large numbers of small ions are replaced by ions with larger radii. As the tetrahedral site A is smaller than that of octahedral site B, A-site will be affected more than B-site. The ionic radii of Mn^{+2}, Zn^{+2} and Fe^{3+} are 0.066 nm, 0.060 nm and 0.049 nm, respectively in the tetrahedral site and 0.083 nm, 0.074 nm and 0.055 nm, respectively in the octahedral site. As the concentration of the Mn^{2+} ion (x) increases

from 0.6 to 0.7, Mn^{2+} ion (0.083 nm) replaces the smaller Fe^{3+} ion (0.055 nm) in the B-site. The doped Zn^{2+} ion (0.060 nm) occupies A-site and the percentage of the Fe^{3+} ion (0.049 nm) increases marginally. This change causes expansion of the B-site and negligible contraction of the A-site. This change gives rise to a marginal increase in the lattice constant values. The lattice constant values for the samples were found to be in conformity with the values reported [16,21]. The XRD data analysis thus confirms formation of monophasic spinel Mn-Zn ferrites. The broadening of XRD peaks indicates formation of fine particle ferrite material.

3.2 Infra Red spectroscopy

Infrared absorption spectra (IR) recorded on the spinel ferrites is known to exhibit six absorption bands. The bands arise from the lattice vibrations of the oxide ions against the cations. The bands in the 300 cm^{-1}–700 cm^{-1} region are assigned to the fundamental vibrations of the crystal lattice. The band around 600 cm^{-1} is attributed to stretching assigned to a vibration of the coordinated group(s) containing the highest valency cation [22]. The bands normally observed are O-H stretching vibration at 3400 cm^{-1}, H-O-H bending vibration at1600 cm^{-1}, O-H-O bending vibration in the range of 900–1000 cm^{-1}, $M_{et} - M_{eo}$ stretching vibration in the range of 600–550 cm^{-1}, $M_{eo} - O$ stretching vibration in the range 450–385 cm^{-1}, and $M_{et} - M_{eo}$ stretching vibration in the range 350–330 cm^{-1}. Where O is oxygen, H – hydrogen, M_{eO} is metal in the octahedral site and M_{et} – is metal in the tetrahedral site. The first three absorption bands observed beyond 1000 cm^{-1} are due to presence of water molecules in the pellets used for measurements. The, $M_{et} - M_{eo}$ stretching vibration in the range of 600–550 cm^{-1} and $M_{eo} - O$ stretching vibration in the range 450 – 385 cm^{-1} are the characteristic lattice vibrations of the oxide ions observed for all spinel ferrite materials. The $M_{et} - M_{eo}$ stretching vibration in the range 350–330 cm^{-1} is normally less intense merges with $M_{eo} - O$ stretching vibration in the range 450–385 cm^{-1} giving a single wide band at 450–330 cm^{-1} as observed in the IR spectra Figure 2.

Figure 2 IR spectra obtained for as prepared (a) $Mn_{0.6}Zn_{0.4}Fe_2O_4$, (b) $Mn_{0.63}Zn_{0.37}Fe_2O_4$, (c) $Mn_{0.65}Zn_{0.35}Fe_2O_4$ (d) $Mn_{0.7}Zn_{0.3}Fe_2O_4$ samples (see online version for colours)

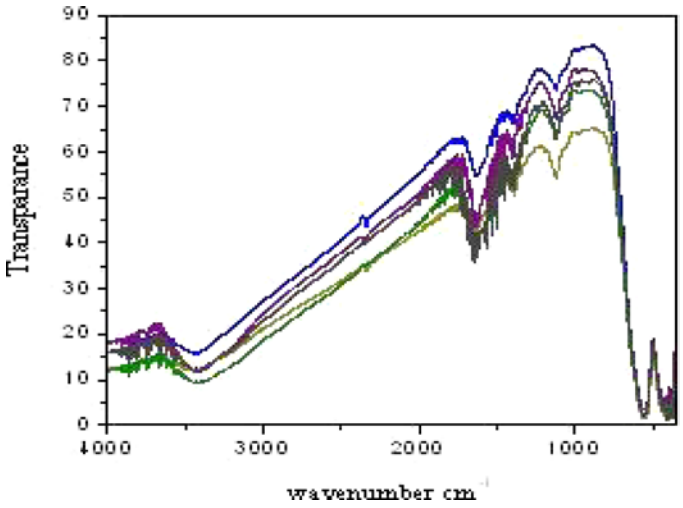

Figure 3 gives the EDS spectra obtained for one of the sample $Mn_{0.60}Zn_{0.40}Fe_2O_4$. Estimated percentage contents of the elements Mn, Zn, Fe and O in the samples obtained with EDS analysis (Table 2 for $Mn_{0.60}Zn_{0.40}Fe_2O_4$) are found to be in good agreement with the theoretically estimated values confirming preservation of stoichiometry [23].

Figure 3 EDS pattern of sample ($Mn_{0.6}Zn_{0.4}Fe_2O_4$)

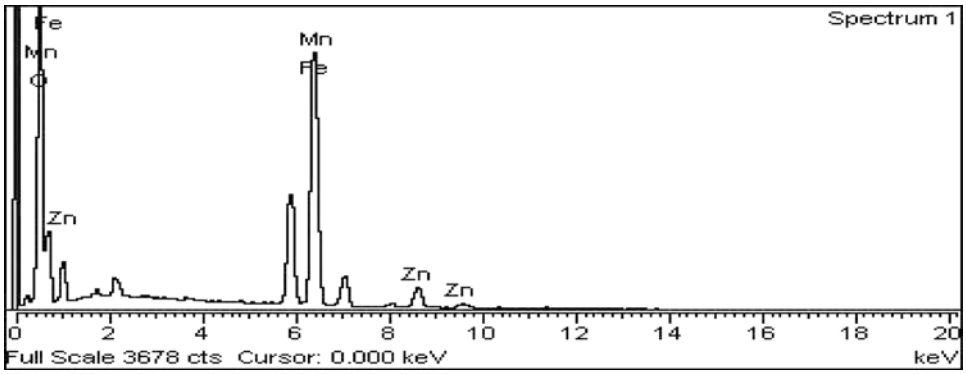

Table 2 EDS results of Sample ($Mn_{0.6}Zn_{0.4}Fe_2O_4$)

Element	O K	Mn K	Fe K	Zn K	Totals
Weight%	24.58	18.55	47.12	9.75	100.00
Atomic%	53.58	11.78	29.43	5.20	–

3.3 Particle size analysis

Figure 4(a) is the TEM micrograph of the nanoparticle $Mn_{0.6}Zn_{0.4}Fe_2O_4$. The size distribution observed in this micrograph is presented in the histogram shown in Figure 4(b). It can be seen that the particle size ranges from as low as 10–35 nm with majority of particles having a size distribution in the range of 15–35 nm. The highest probability is observed for particles with grain size in the range of 25–30 nm. The 220, 311, 400, 511, 440 reflection peaks in the XRD patterns of all the samples were used for calculating particle size by Scherrer formula. The average particle sizes calculated for the entire range of samples are tabulated in Table 3. The results show that the sizes of the particles obtained are in the range of 24.67–41.67 nm. The marginal difference observed in the particle size of sample $Mn_{0.6}Zn_{0.4}Fe_2O_4$ obtained by two different methods may be attributed to non consideration of correction factors in the Scherrer's formula and other instrumental errors. However both the TEM and XRD data on particle size provide convincing evidence about formation of polycrystalline nanoparticle samples.

Table 3 The particle size obtained for samples $Mn_xZn_{(1-x)}Fe_2O_4$ using Scherrer formula

Mn Conc. x	0.60	0.63	0.65	0.67	0.70
Particle size (nm)	38.62	33.62	24.67	41.67	29.75

Figure 4 (a) The TEM micrograph; (b) particle size distribution of sample $Mn_{0.6}Zn_{0.4}Fe_2O_4$) (see online version for colours)

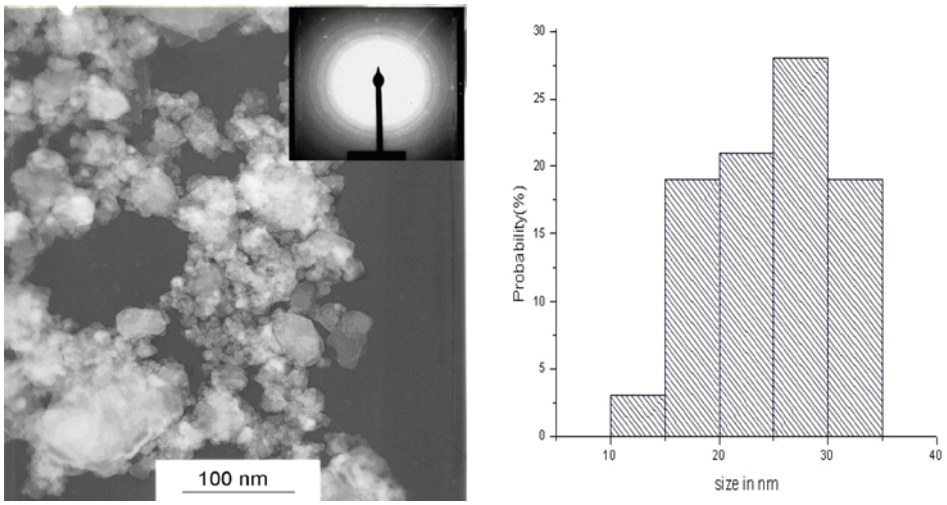

(a) (b)

3.4 Magnetic measurements

3.4.1 Saturation magnetisation

In spinel Mn-Zn ferrite metal ions and Fe ions are uniformly distributed over A and B sites. Zn^{+2} and Mn^{+2} partly occupy tetrahedral and octahedral sites whereas Fe^{+3} occupy both tetrahedral and octahedral sites. The magnetic super exchange interactions A-A, B-B and A-B are of indirect type and mediated via oxygen ion surrounded by 1 A cation and 3 B cations. Interaction energy between the two ions Mn^{+2} and Zn^{+2} depends upon their distance from oxygen ions and the angle between Mn^{+2}-O-Zn^{+2} ions. Among the three antiferromagnetic interactions A-A, B-B and A-B the interaction A-B is the strongest due to fairly higher angle and the resultant saturation magnetisation comes from this interaction given by $Ms = |M_B - M_A|$. Interactions of the type A-A, A-B and B-B type are known to exhibit canted spin structures for certain ratios of exchange coupling constants thus cation distribution plays an important role is deciding the saturation magnetisation of the particle core.

The variation of saturation magnetisation ($\mathbf{M_s}$) with Mn concentration 'x' in the sample is shown in Figure 5. $\mathbf{M_s}$ is found to largely depend on the Mn concentration of the sample. For soft crystalline materials the magnetic behaviour is dominated by the magnetocrystalline anisotropy which can be controlled by the material composition and thermo-mechanical procedures applied to the sample. The magneto crystalline anisotropy consisting of surface spin isotropy and crystalline or shape anisotropy, manifest in the $\mathbf{M_s}$ of the sample. Moreover in nanomaterials the grain size which depends on the method of preparation, giving rise to surface effects and finite size effects due to changing surface to volume ratio, is a highly unpredictable parameter that brings noticeable changes in the material magnetic properties. The over all high values of saturation magnetisation suggests that the thickness of the nonuniform disordered shell is small thereby increasing the contribution from the of the particle core.

Figure 5 Variation of saturation magnetisation with Mn conc. x obtained from hysteresis loop tracer (see online version for colours)

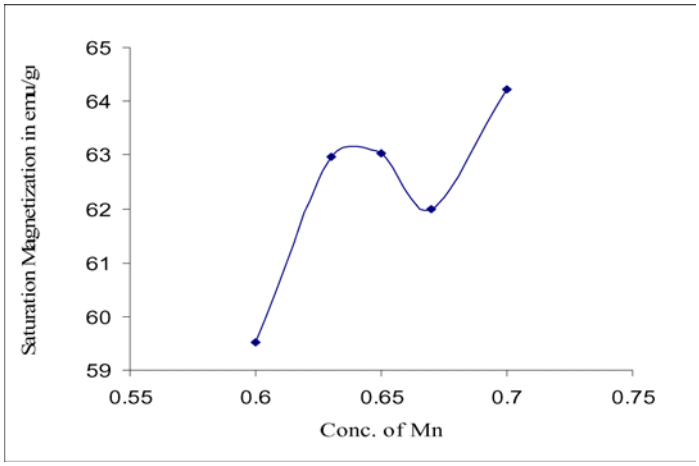

3.4.2 Low temperature Magnetic (SQUID) measurements

Low temperature magnetic properties of $Mn_{0.67}Zn_{0.33}Fe_2O_4$ nanoparticles were studied by SQUID magnetometer. Figure 6(a) shows temperature dependence of magnetisation of $Mn_{0.67}Zn_{0.33}Fe_2O_4$. The $Mn_{0.67}Zn_{0.33}Fe_2O_4$ nanoparticles for temperature-dependent magnetisation study were cooled from room temperature to 5 K in absence of magnetic field. The magnetisation of the nanoparticles was measured after application of a magnetic field of 100 Oe at 5 K. The magnetisation of the $Mn_{0.67}Zn_{0.33}Fe_2O_4$ nanoparticles remains at zero till the sample temperature is near about 25 K this happens as the applied magnetic field is not strong enough to overcome the magnetic anisotropy alone in the sample. When the temperature rises, the magnetic anisotropy in some nanoparticles is overcome due to thermal activation. The magnetisation directions of these nanoparticles align with the applied field, similar to a typical paramagnetic material. The magnetisation increases with temperature and a maximum is reached at around 250 K which is the blocking temperature. Beyond this temperature the magnetisation is found to decrease with increasing temperature. When the temperature reaches the blocking temperature, the magnetisation directions of all the nanoparticles point towards the field direction and gives a high magnetisation [24,25]. Figure 6(b) shows the field dependence of magnetisation of the same sample $Mn_{0.67}Zn_{0.33}Fe_2O_4$ at 35 K. The plot displays that the magnetisation of the superparamagnetic nanoparticles changes its direction in unison with the direction reversal of the applied magnetic field. A high saturation magnetisation of 120 emu/g at this temperature is obtained for the sample at 50,000 Oe.

3.4.3 Room temperature Magnetic properties (VSM)

Room temperature measurements of magnetic properties were carried out on VSM. The typical hysteresis loop obtained for sample $Mn_{0.65}Zn_{0.35}Fe_2O_4$ from the data collected is shown in Figure 7. Small area under loop ensures low hysteress loss and low eddy currents. It can be seen that the contribution to saturation magnetisation coming from the disordered shell is quite small.

Figure 6 (a) Low temperature dependence of magnetisation (b) field dependent magnetisation of as prepared sample $Mn_{0.67}Zn_{0.33}Fe_2O_4$ at low temperature

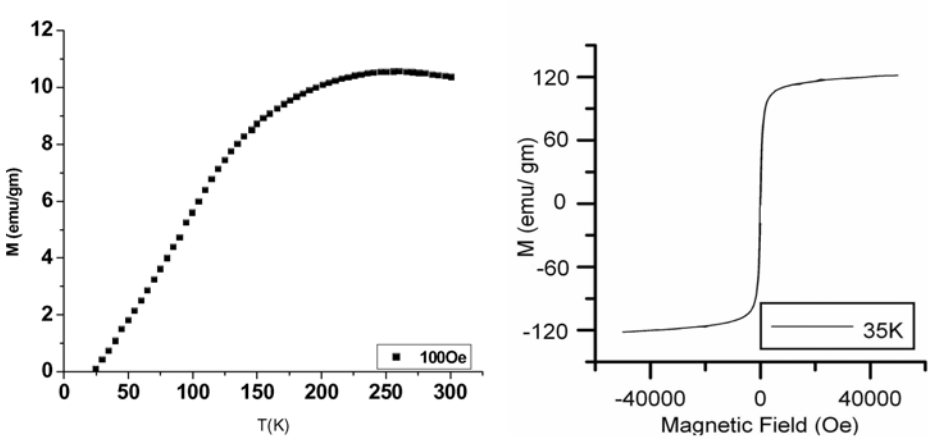

Figure 7 Hysteresis loop for sample $Mn_{0.65}Zn_{0.35}Fe_2O_4$ obtained from VSM data

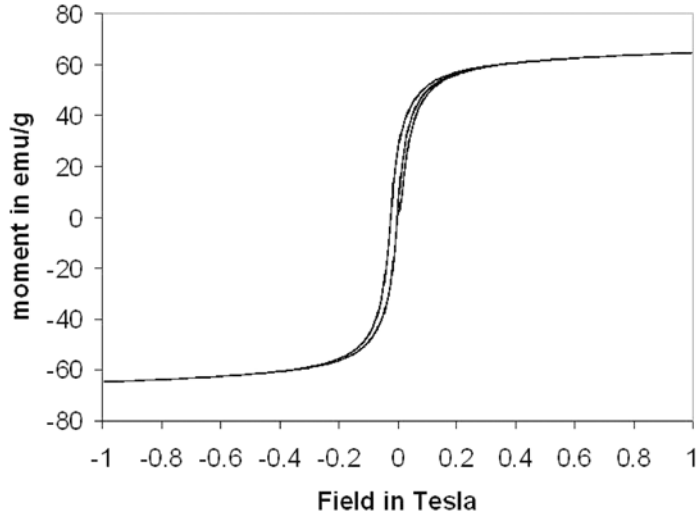

Table 4 Room temperature variation of magnetic properties $\mathbf{M_r}$, $\mathbf{M_s}$, $\mathbf{M_r/M_s}$, $\mathbf{H_c}$ with Mn conc.

Mn Conc. x	*Retentivity* $\boldsymbol{M_r}$ emu/g	*Saturation magnetisation* $\boldsymbol{M_s}$ emu/g	*Squareness* $\boldsymbol{M_r/M_s}$	*Coercivity* $\boldsymbol{H_c}$ Oe
0.60	30.74	56.20	0.5470	23.57
0.63	14.33	62.21	0.2304	0.56
0.65	5.32	63.58	0.0837	86
0.67	14.33	58.31	0.2457	14.6
0.70	1.17	64.23	0.0182	1.06

The VSM data collected on nanoparticle $Mn_xZn_{(1-x)}Fe_2O_4$ samples are listed in Table 4. The values of squareness ($\mathbf{M_r/M_s}$) for all the samples are found vary between 0.0182 and 0.547. A lowest value of 0.0182 is obtained for sample with x = 0.7. Coercivity and retaintivity varies greatly with grain size and is evident from similar variations observed in Table 3. The disordered shell which contributes very little to saturation magnetisation at normal temperatures and Mn content in the sample are other major factors influencing these properties. As the samples are polycrystalline nanomaterials, the magnitude of contributions resulting from particles of different sizes will be a function of their local population in the sample. However the samples with x = 0.65, 0.7 give very low values for ($\mathbf{M_r/M_s}$) due to presence of large number of superparamagnetic grains in the samples and as such exhibit superparamagnetism.

Table 5 Variation of Curie temperature with Mn Conc. 'x'

Mn Conc. x	0.60	0.63	0.65	0.67	0.70
T_c in ^oC	240	246	330	285	353

Figure 8 is a typical AC susceptibility curve obtained on pulsed field magnetisation setup for sample $Mn_{0.65}Zn_{0.35}Fe_2O_4$ showing variation of specific magnetisation with temperature. Table 5 shows variation of Curie temperature T_c with Mn concentration x as obtained from AC susceptibility measurements made on the samples. Obviously the T_c is expected to depend on the magnetic properties of the samples. The magnetic properties of a sample depend on the domain structure of the nanoparticles and are driven by material particle size. The magnetisation/demagnetisation due to domain wall movement requires lower energy compared to that required for domain rotation [26,27], hence $\mathbf{M_r}$ and $\mathbf{H_c}$ values in superparamagnetic (SPM) and multi domain (MD) grains are normally lower than those of single domain (SD) grains. However in nanoparticle grains under investigation the $\mathbf{M_r}$ and $\mathbf{H_c}$ values remain low but the material appears to exhibit single domain behaviour as observed from the AC susceptibility measurements. This may be due to the composition of the particles which contributes as aligned core enclosed in a shell of disordered spins.

Figure 8 Curve obtained for sample $Mn_{0.65}Zn_{0.35}Fe_2O_4$ showing variation of specific magnetisation (AC susceptibility) with temperature (see online version for colours)

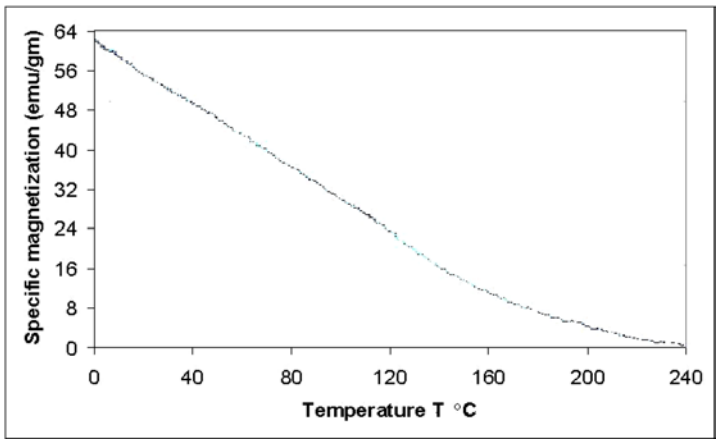

3.5 Density

The variation of density of the sample was determined by pycknometric method. The density of the samples was found to be high and ranged between 3.13 g/cc to 3.35 g/cc. It may be seen that grain size follows a reverse trend when compared with saturation magnetisation, Curie temperature and density which follow a similar trend with variation of Mn concentration in the sample. Saturation magnetisation, density and T_c is found to share a inverse relation with the grain size of the nanoparticle ferrite. The density is found to be higher for samples with lower grain size which is obvious as the sample would be more compact.

Figure 9 Variation of density with Mn concentration x obtained by pycknometric method (see online version for colours)

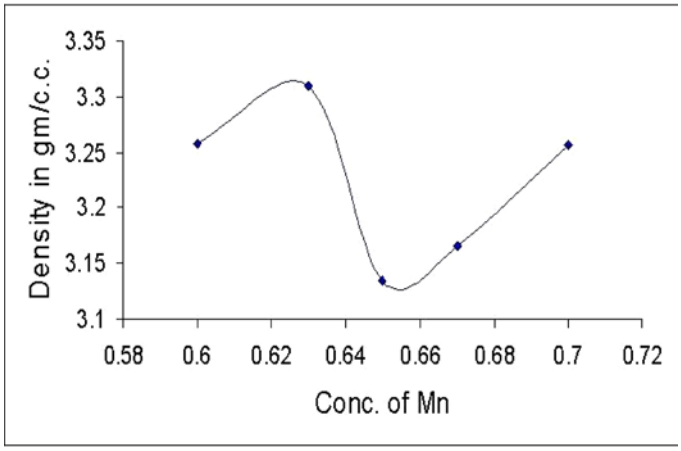

4 Conclusion

Nanoparticle $Mn_xZn_{(1-x)}Fe_2O_4$ with x = 0.6, 0.63, 0.65, 0.67, 0.7 materials were prepared by nitrilotriacetate precursor method employing microwave assisted auto-combustion synthesis. The particle size distribution of the nanoparticles was in the range of 10–41.67 nm. The low temperature magnetic measurements (SQUID) made on the sample $Mn_{0.67}Zn_{0.33}Fe_2O_4$ and room temperature magnetic measurements (VSM) indicate that samples exhibit superparamagnetic behaviour. One is justified in categorising the nanoferrite as low hysteresis loss materials due to low values of $\mathbf{M_r}$, $\mathbf{H_c}$ and high values of $\mathbf{M_s}$ exhibited by the samples. $\mathbf{M_r}$, $\mathbf{M_s}$, $\mathbf{M_r/M_s}$, $\mathbf{H_c}$ is found to depend on the Mn concentration and particle size of the nanomaterial. The density of the materials was between 3.13 g/cc to 3.35 g/cc Saturation magnetisation $\mathbf{M_s}$ Curie temperature $\mathbf{T_c}$ and density of the sample exhibiting similar behaviour depend on Mn concentration x in the sample and particle size of the sample. The saturation magnetisation $\mathbf{M_s}$ Curie temperature $\mathbf{T_c}$ and density following similar trends are found to dependent inversely on the particle size of the samples. Samples with low particle size are seen to display higher saturation magnetisation values $\mathbf{M_s}$, curie temperature $\mathbf{T_c}$ and density where as samples with larger particle size display lower values.

Although the nanosamples are polycrystalline in nature the study shows that the grain boundary thickness or the thickness of the disordered shell enclosing aligned core of the particle is larger in bigger particles then in smaller ones. Thus higher values of saturation magnetisation are observed for samples with small particle size.

It is interesting to see that the range of saturation magnetisation values is higher for samples prepared by this method this is due to formation of the samples at low temperature. When preparation temperature is low the evaporation of Zn from the grain boundary is low and this reduces the thickness of disordered shell and thus the magnetic properties are enhanced.

These materials could be good candidates for high performance in nano and bulk applications as material with enhanced magnetic properties, lower porosity and small grain size may be easily obtained by sintering the green bodies prepared from nanoparticles. Bulk material obtained by sintering of microwave synthesised nanoparticles is known to retain the majority of the properties they exhibit in nanoform [28–31].

References

1 McCurrie, R.A. (1994) *Ferromagnetic Materials Structure and Properties*, Academic, London, pp.123–188.

2 Oliver, S.A., Hamdeh, H.H. and Ho, J.C. (1999) 'Localized spin canting in partially inverted $ZnFe_2O_4$ fine powders', *Phys. Rev. B*, Vol. 60, pp.3400.

3 Chinnasamy, C.N., Narayanasamy, A., Ponpandian, N., Chattopadhyay, K., Shimoda, K., Jayadevan, B., Tohji, K., Nakatsuka, K., Furubayashi, T. and Nakatani, I. (2001) 'Mixed spinel structure in nanocrystalline $NiFe_2O_4$', *Phys. Rev. B*, Vol. 63, pp.184108.

4 Muroi, M., Street, R., McCormick, P.G. and Amighian, J. (2001) 'Magnetic properties of ultrafine $MnFe_2O_4$ powders prepared by mechanochemical processing', *Phys. Rev. B*, Vol. 63, pp.184414.

5 Sepelak, V., Baabe, D., Mienert, D., Litterst, F.J. and Becker, K.D. (2003) 'Enhanced magnetisation in nanocrystalline high-energy milled $MgFe_2O_4$', *Scr. Mater*., Vol. 48, pp.961.

6 Kodama, R.H., Berkowitz, A.E., McNiff Jr., E.J. and Foner, S. (1996) 'Surface spin disorder in $NiFe_2O_4$ nanoparticles', *Phy. Rev. Lett*., Vol.77, pp.394.

7 Pajic, D., Zadro, K., Vandenberghe, R.E. and Nedkov, I. (2004) 'Superparamagnetic relaxation in $Cu_xFe_{3-x}O_4$ (x=0.5 and x=1) nanoparticles', *J. Magn. Magn. Mater*., Vol. 281, pp.353.

8 CHkoundali, S., Ammar, S., Jouini, N., Fievet, F., Molinie, P., Danot, M., Villain, F. and Greneche, J.M. (2004) 'Nickel ferrite nanoparticles: elaboration in polyol medium via hydrolysis, and magnetic properties', *J. Phys.: Condens. Matter*, Vol. 16, pp.4357.

9 Li, F.S., Wang, L., Wang, J.B., Zhou, Q.G., Zhou, X.Z., Kunkel, H.P. and Williams, G. (2004) 'Site preference of Fe in nanoparticles of $ZnFe_2O_4$', *J. Magn. Magn. Mater.*, Vol. 268, pp.332.

10 Battle, X. and Labarta, A. (2002) 'Finite-size effects in fine particles: magnetic and transport properties', *J. Phys. D: Appl. Phys*., Vol. 35, No. 6, pp.R15–R42.

11 Hariharan, S. and Gass, J. (2005) 'Superparamagnetism and magnetocaloric effect (MCE) in functional magnetic nanostructures', *Rev. Adv. Mater. Sci*., Vol. 10, pp.398–402.

12 Liu, C. and John Zhang, Z. (2001) 'Size-dependent superparamagnetic properties of Mn spinel ferrite nanoparticles synthesized from reverse micelles', *Chem. Mater*., Vol. 13,pp.2092–2096.

13 Raikher, Y. and Perzynski, R. (2005) *Surface Effects in Magnetic Nanoparticles*, Edited by *D. Fiorani* (Springer, New York).

14 Aquino, R., Depeyrot, J., Sousa, M.H., Tourinho, F.A., Dubois, E. and Perzynski, R. (2005) 'Magnetization temperature dependence and freezing of surface spins in magnetic fluids based on ferrite nanoparticles', *Phys. Rev. B*, Vol. 72, pp.184435.

15 Parvatheeswara Rao, B. and Caltun, O.F. (2006) 'Synthesis and characterization of some ferrite nanoparticles', *J. Optoelectron. Adv. Mater.*, Vol. 8, No. 3, pp.991–994.

16 Tangsali, R.B., Keluskar, S.H., Naik, G.K. and Budkuley, J.S. (2004) 'Effect of sintering conditions on magnetic properties of nanoparticle Mn-Zn ferrite synthesized with nitrilotriacetate precursor method', *Int. J. Nanosci.*, Vol. 3, Nos. 4–5, pp.1–9.

17 Tangsali, R.B., Keluskar, S.H., Naik, G.K. and Budkuley, J.S. (2007) 'Effect of sintering conditions on resistivity of nanoparticle Mn-Zn ferrite prepared by nitrilotriacetate precursor method', *J. Mater. Sci*., Vol. 42, pp.878–882.

18 Oliver Kappe, C. and Stadler, A. (2005) *Microwaves in Organic and Medicinal Chemistry*, Wiley-VCH, Weinheim.

19 Loupy, A. (Ed.) (2006) *Microwaves in Organic Synthesis*, Wiley-VCH, Weinheim.

20 Rath, C., Anand, S. and Das, R.P. (2002) 'Dependence on cation distribution of particle size, lattice parameter, and magnetic properties in nanosize Mn–Zn ferrite', *J. Appl. Phys.*, Vol. 91, pp.2211.

21 Iyer, R., Desai, R. and Upadhyay, R.V. (2009) 'Low temperature synthesis of nanosized $Mn_{1-x}Zn_xFe_2O_4$ ferrites and their characterizations', *Bull. Mater. Sci*., Indian Academy of Sciences, Vol. 32, No. 2, April, pp.141–147.

22 Tarte, P. and Preudhomme, J. (1971) 'Infrared studies of spinels – I: A critical discussion of the actual interpretations', *Spectrochim. Acta, Part A*, Vol. 27, pp.961–968.

23 Son, S., Swaminathan, R. and McHenry, M.E. (2003) 'Structure and magnetic properties of rf thermally plasma synthesized Mn and Mn-Zn ferrite nanoparticle', *J. Appl. Phys.*, Vol. 93, pp.7495.

24 Liu, C., Zou, B., Rondinonen, A.J. and John Zhang, Z. (2000) 'Reverse micelle synthesis and characterization of superparamagnetic $MnFe_2O_4$ spinel ferrite nanocrystallites', *J. Phys. Chem. B*, Vol. 104, pp.1141–1145.

25 Chandana, R., Mishra, N.C., Anand, S., Das, R.P., Sahu, K.K., Upadhaya, C. and Verma, H.L. (2000) 'Appearance of superparamagnetism on heating nanosize $Mn_{0.65}Zn_{0.35}Fe_2O_4$', *Appl. Phys. Lett.*, Vol. 76, No. 4, pp.475–477.

26 Leslie-Pelecky, D.L. and Rieke, R.D. (1996) 'Magnetic properties of nanostructured materials', *Chem. Mater.*, Vol. 8, No. 8, pp.1770–1783.

27 Liu, C. and John Zhang, Z. (2001) 'Size-dependent superparamagnetic properties of Mn spinel ferrite nanoparticles synthesized from reverse micelles', *Chem. Mater.*, Vol. 13, pp.2092–2096.

28 Ganesh, I., Johnson, R., Rao, G.V.N., Mahajan, Y.R., Madavendra, S.S. and Reddy, B.M. (2005) 'Microwave-assisted combustion synthesis of nanocrystalline$MgAl_2O_4$ spinel powder', *Ceram. Int.*, Vol. 31, pp.67–74.

29 Ganesh, I., Srinivas, B., Johnson, R., Saha, B.P. and Mahajan, Y.R. (2002) 'Effect of fuel type on morphology and reactivity of combustion synthesized $MgAl_2O_4$ powders', *Br. Ceram. Trans*., Vol. 101, No. 6, pp.247–256.

30 Ganesh, I., Srinivas, B., Johnson, R., Rao, G.V.N. and Mahajan, Y.R. (2003) 'Effect of preparation method on sinterability and properties of nanocrystalline$MgAl_2O_4$ and ZrO^{2-} $MgAl_2O_4$ materials', *Br. Ceram. Trans*., Vol. 102, No. 3, pp.119–128.

31 Verma, S., Joy, P.A., Khollam, Y.B., Potdar, H.S. and Deshpande, S.B. (2004) 'Synthesis of nanosized $MgFe_2O_4$ powders by microwave hydrothermal method', *Mater. Lett.*, Vol. 58, No. 6, pp.1092–1095.